Applied Surface Science 412 (2017) 554–558

Contents lists available at ScienceDirect

Applied Surface Science

journal homepage: www.elsevier.com/locate/apsusc

Full length article

Photodetectors for weak-signal detection fabricated from ZnO:(Li,N) films

G.H. He[a,b], H. Zhou[c], H. Shen[a], Y.J. Lu[d], H.Q. Wang[c], J.C. Zheng[c], B.H. Li[a], C.X. Shan[a,d,*], D.Z. Shen[a]

[a] State Key Laboratory of Luminescence and Applications, Changchun Institute of Optics, Fine Mechanics and Physics, Chinese Academy of Sciences Changchun 130033, China
[b] University of Chinese Academy of Sciences, Beijing 100049, China
[c] Key Laboratory of Semiconductors and Applications of Fujian Province, Collaborative Innovation Center for Optoelectronic Semiconductors and Efficient Devices, Department of Physics, Xiamen University, Xiamen 361005, China
[d] Henan Key Laboratory of Diamond Optoelectronic Materials and Devices, School of Physics and Engineering, Zhengzhou University, Zhengzhou 450001, China

ARTICLE INFO

Article history:
Received 21 November 2016
Received in revised form 18 March 2017
Accepted 31 March 2017
Available online 2 April 2017

Keywords:
Photodetector
ZnO
Detectivity
Noise equivalent power

ABSTRACT

ZnO films with carrier concentration as low as 5.0×10^{13} cm^{-3} have been prepared via a lithium and nitrogen codoping method, and ultraviolet photodetectors have been fabricated from the films. The photodetectors can be used to detect weak signals with power density as low as 20 nw/cm^2, and the detectivity and noise equivalent power of the photodetector can reach 3.60×10^{15} cmHz$^{1/2}$/W and 6.67×10^{-18} W^{-1}, respectively, both of which are amongst the best values ever reported for ZnO based photodetectors. The high-performance of the photodetector can be attributed to the relatively low carrier concentration of the ZnO:(Li,N) films.

1. Introduction

As a type of electronic devices for sensing light, photodetectors have a variety of potential applications in both civil and military fields such as sensors, radiation calibration and monitoring, astronomical studies, optical communication, missile launch detection, and so on [1–6]. Because of the above potential applications, the development of photodetectors is very important and urgent. ZnO is a wide band gap (3.37 eV at room temperature) semiconductor, which makes it suitable for applications in short-wavelength ultraviolet (UV) optoelectronic devices, such as photodetectors, light-emitting devices, lasers, and so on [7–12]. So far various typed ZnO photodetectors, such as Schottky photodiodes, metal-semiconductor-metal (MSM) photodetectors [13–15] and *p-n* junction photodiodes [16,17] have been demonstrated. However, the performance of the photodetector devices is far behind expectation. Especially ZnO photodetectors that can be employed to detect weak signals are still eagerly wanted, which has been one of the largest obstacles for the future applications of ZnO based UV photodetectors.

In this paper, high-resistance ZnO films have been prepared by using lithium and nitrogen codoping method, and the carrier concentration of the films is 5.0×10^{13} cm^{-3}, which is over four orders of magnitude smaller than that of undoped ZnO films (5.7×10^{17} cm^{-3}). The relatively low carrier concentration is favorable for the realization of photodetectors that can be employed for weak signal detection. Photodetectors fabricated from the films show capability to detect weak signals as low as 20 nw/cm^2, and the detectivity and noise equivalent power (*NEP*) of the photodetector can reach 3.60×10^{15} cmHz$^{1/2}$/W and 6.67×10^{-18} W^{-1}, respectively, both of which are amongst the best values ever reported for ZnO photodetectors.

2. Experiments

The Li,N codoped ZnO (ZnO:(Li,N)) thin films employed as the active layer of the photodetector were grown on *c*-plane sapphire by plasma assisted molecular beam epitaxy technique. Prior to the growth, the sapphire substrates were treated at 650 °C for 30 min to

* Corresponding author at: State Key Laboratory of Luminescence and Applications, Changchun Institute of Optics, Fine Mechanics and Physics, Chinese Academy of Sciences Changchun 130033, China.
E-mail address: shancx@ciomp.ac.cn (C.X. Shan).

http://dx.doi.org/10.1016/j.apsusc.2017.03.295
0169-4332/

clean the surface. Elemental zinc (6N) and lithium (3N) contained in Knudsen effusion cells were used as Zn and Li source. Oxygen (6N) cracked via a radio-frequency atom source was used as O source, nitric oxide (NO) gas (6N) cracked via a radio-frequency atom source was used as N and O source for the growth of the ZnO:(Li,N) films. During the growth progress, the substrate temperature was fixed at 650 °C, and the pressure in the growth chamber at 2×10^{-5} mbar. To fabricate ZnO:(Li,N) based photodetectors, a thin Au layer was deposited onto the films by vacuum evaporation method, and interdigital electrodes were configured on the films via a photolithography and wet etching process.

The crystalline properties of the ZnO:(Li,N) films were characterized by a Bruker D8 Discover x-ray diffractometer (XRD) with Cu Kα (λ = 1.54 Å) as the radiation source. Electrical properties of the films were measured in a Hall measurement system (Lakeshore 7707) under Van der Pauw configuration. The surface morphology of the ZnO:(Li,N) films was characterized by a Hitachi S4800 field-emission scanning electron microscope (SEM). The chemical bonding states in the ZnO:(Li,N) films was analyzed in an AXIS Ultra 'DLD' X-ray photoelectron spectrometer (XPS). X-ray absorption near edge structure (XANES) spectra of O K-edge in the ZnO:(Li,N) films were obtained at the Photoemission Spectroscopy station (Beam line 4B9B) of Beijing Synchrotron Radiation Facility. Extended x-ray absorption fine structure (EXAFS) spectra of Zn K-edge in the samples were collected at the X-ray Absorption Fine Structure station (Beam line 14 W1) of Shanghai Synchrotron Radiation Facility using the fluorescence mode at room temperature. The acceptor state of the ZnO:(Li,N) films has been studied by investigating the local electronic structures of the films using x-ray absorption fine structure (XAFS) based on synchrotron radiation source, and such a technique has been employed to study the local electronic structures of ZnO [18,19]. The current-voltage (I–V) properties of the devices were measured using a semiconductor parameter analyzer (Keithely 2200).

3. Results and discussion

Fig. 1(a) shows the XRD patterns of the undoped ZnO and ZnO:(Li,N) films, from which one can see that for both cases, besides the diffraction from the sapphire substrate, a strong peak can be observed, which can be indexed to the diffraction from (002) facet of ZnO. The strong (002) diffraction peak indicates that both the ZnO:(Li,N) films and undoped ZnO films are crystallized in wurtzite structure. The plan-view SEM images of the ZnO:(Li,N) films are displayed in Figs. 1(b). One can see that the ZnO:(Li,N) films have a smooth surface.

Under dark conditions, the electrical conductivity of a semiconductor can be expressed by the following formula:

$$\sigma_0 = q(n_0 \mu_n + p_0 \mu_p) \quad (1)$$

In which q is the electron charge; n_0 and p_0 are the equilibrium carrier concentration; μ_n, μ_p is the mobility of the electrons and holes, respectively. When the semiconductor is exposed to illumination, Δn and Δp are the number of the photon-generated carriers. The σ_0 become σ

$$\sigma = q(n\mu_n + p\mu_p) \quad (2)$$

$n = n_0 + \Delta n$ and $p = p_0 + \Delta p$. We can get the photoconduction $\Delta\sigma = q(\Delta n\mu_n + \Delta p\mu_p)$. The relative value is

$$\Delta\sigma/\sigma_0 = (\Delta n\mu_n + \Delta p\mu_p)/(n_0 \mu_n + p_0 \mu_p) \quad (3)$$

From the above formula, one can see that to get high photoconductivity, the n_0 and p_0 must be as small as possible. Table 1 shows the electrical properties of the undoped and ZnO:(Li,N) films. The Hall mobility of the ZnO:(Li,N) is smaller than the undoped ZnO film, but the carrier concentration in the doped films is as low as 5.0×10^{13} cm^{-3}, which is about four order of magnitude lower than in the undoped ZnO films (5.7×10^{17} cm^{-3}). The reason for the decreased carrier concentration in the ZnO:(Li,N) films will be depicted below.

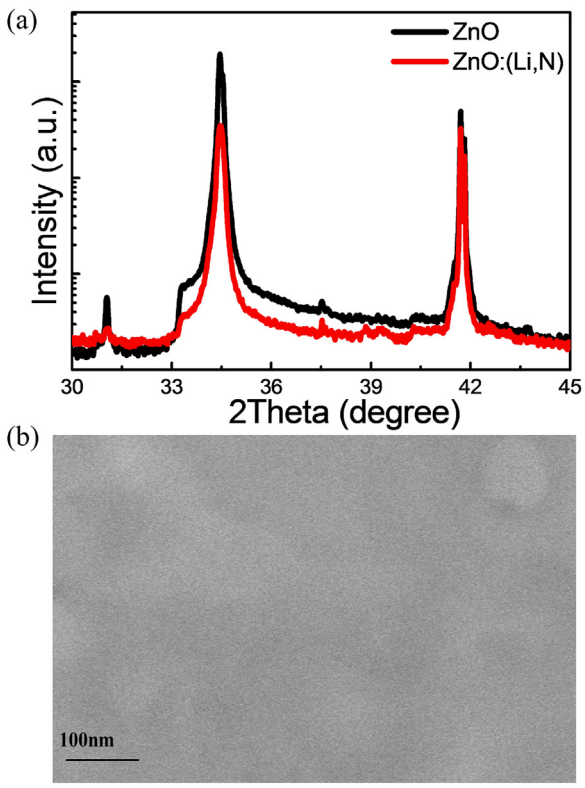

Fig. 1. (a) XRD patterns of the undoped ZnO and ZnO:(Li,N) films. (b) Plan-view SEM images of the ZnO:(Li,N) films.

Table 1
Hall data of the undoped ZnO and ZnO:(Li,N) films.

Sample	Conductivity	Hall mobility (cm^2/Vs)	Carrier concentration (cm^{-3})	Resistivity (Ωcm)
ZnO	n	20.6	5.7×10^{17}	5.29×10^{-1}
ZnO:(Li,N)	n	3.5	5.0×10^{13}	9.81×10^{3}

Fig. 2 shows the XPS spectrum of the ZnO:(Li,N) film, and the composition of the Li and N in the ZnO:(Li,N) films determined by XPS is around 3.46% and 0.49%, respectively. In Fig. 2(a), a Li 1s peak is evidenced at 55.3 eV, which is close to the binding energy of Li in Li—N bonds (55.0 eV) and Li—O bonds (55.6 eV) [20,21]. No signal from Li_i (52.9 eV) can be found, revealing that the incorporated Li may occupy Zn sites to form the acceptors Li_{Zn} bonding with N and/or O, while the Li_i that is frequently observed in Li doped ZnO has not been observed in our case. The N1s spectrum shown in Fig. 2(b) is located at 398.8 eV, which is close to the binding energy of Li—N bonds. One can deduce from the above data that Li—N bonds form in the ZnO:(Li,N) films. Thus, it is rational to speculate from the XPS data that the acceptor formed in ZnO:(Li,N) film may be the Li—N complex containing Li_{Zn} and N_O.

In order to further prove the above speculation, the O K-edge XANES absorption spectra of the ZnO:(Li,N), ZnO:N, ZnO:Li, and ZnO films have been measured, as shown in Fig. 3(a). There are three main bulge areas marked A, B, C in the spectra. The most distinctive features from the four samples with different doping status appear in the C area, which is located at approximately from 539 eV

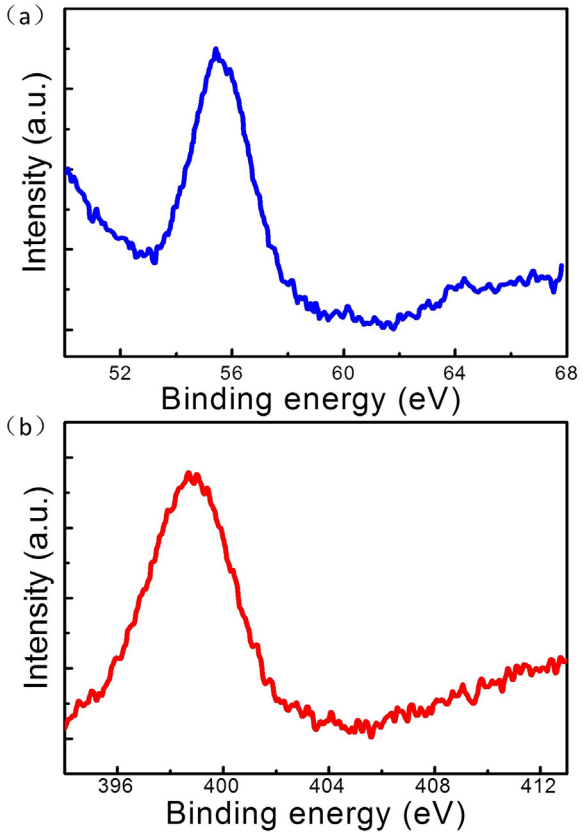

Fig. 2. XPS spectra of Li 1s (a) and N 1s (b) in ZnO:(Li,N) films.

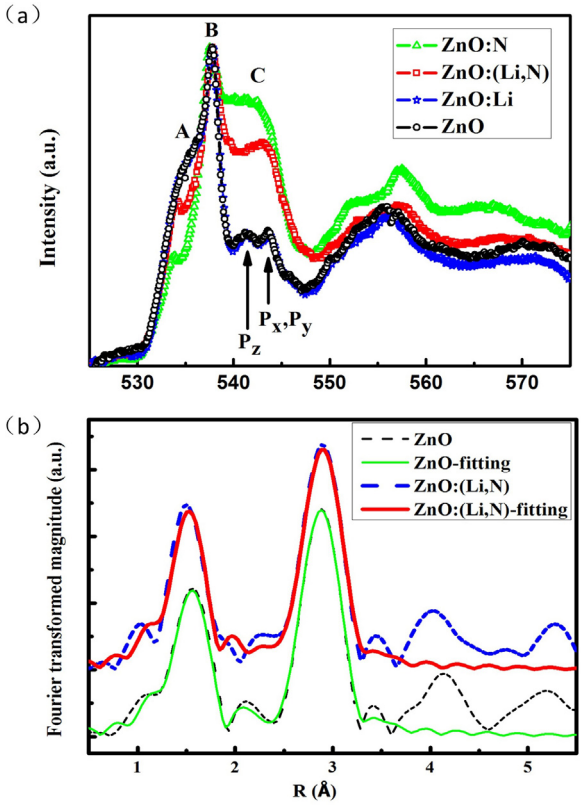

Fig. 3. (a)O K-edge XANES spectra of the ZnO:(Li, N), ZnO:N, ZnO:Li and undoped ZnO films. (b) Fourier transformed Zn K-edge EXAFS data of the ZnO:(Li,N) and undoped ZnO films.

Table 2
Bond lengths of the ZnO:(Li,N) and undoped ZnO films from Zn K-edge EXAFS analysis.

Sample	Zn—O bond length (Å)	Zn—Zn bond length (Å)
ZnO	1.972	3.190
ZnO:(Li,N)	1.943	3.153

to 550 eV, and is mainly attributed to O 2*p* hybridized with Zn 4*p* states in the films [22]. The C area is composed of two small bulges, originated from O p_z and p_x (p_y) orbits, thus it can reflect the change of O *p* orbit directly. As illustrated in Fig. 3(a), the intensity of C area in the ZnO:N film is larger than that in undoped ZnO films. Such a phenomenon may be caused by the fact that some O positions have been occupied by N, which will lead to the decrease of electron number, thus the increased absorption intensity of the O *p* orbit has been resulted for the nitrogen doped ZnO films compared with the undoped ones. On the other hand, as Li doping does not influence the O *p* orbit, the C area in ZnO:Li shows no obvious change from that in the undoped ZnO films. The intensity of C area in the ZnO:(Li,N) lies between that of ZnO:N and ZnO films, which may be due to the fact that the Li bonding with N will partially offset the impact of O *p* orbit caused by the N occupying O site. The above results are consistent with the speculation shown in the XPS data that N has been bonded with Li in the ZnO:(Li,N) films.

The Zn K-edge EXAFS spectra of the samples were analyzed by Athena V0.8.056, Artemis V0.8.012 with the IFEFFIT package version 1.2.11 [23–25]. Both the experimental results and the fitting curves are displayed in R-space and provided in Fig. 3(b) and the detailed analysis procedure can be found elsewhere [26]. In the simulation of the ZnO:(Li,N) film, Li and N are assumed to substitute for the Zn and O sites, respectively. The dashed lines in Fig. 3(b) show the Fourier transformed experimental EXAFS data of the undoped ZnO films (thin dashed line) and ZnO:(Li,N) films (thick dashed line). The solid lines are Artemis fitting data, well fitted to the experimental data. The first shell of the radial distribution function indicates the position of the Zn—O bond distance, and the second shell peak denotes a combination of Zn—Zn bond distances. The best fitting results of the bond length are presented in Fig. 3(b) and the bond length data obtained via the fitting are summarized in Table 2. The undoped ZnO film has Zn—O and Zn—Zn bond length of 1.972 Å and 3.190 Å, respectively. The bond length of Zn—O in the ZnO:(Li,N) film is shorter than that in the undoped ZnO film. One may speculate that the length of Zn—Zn bonds will be increased if $(N_2)_O$ or Li_i is dominant because both of them will occupy larger space than a single O atom, and the Zn atoms will then be pushed away from their original sites. The fact that the Zn—Zn bonding length has been decreased, instead indicates that N and Li mainly exist in the forms of N_O and Li_{Zn}. These findings further confirm the formation of Li—N complex acceptors have formed in the ZnO:(Li,N) films. The low carrier concentration may be caused by the compensation of the N_O and Li_{Zn} acceptors to the residual donors in the ZnO films, which is favorable for weak signal detection if a photodetector can be fabricated from the ZnO films.

The schematic illustration of the photodetector fabricated from the ZnO:(Li,N) films is shown in Fig. 4(a). The interdigital Au electrodes are consisted of 12 fingers for each electrode, the fingers are 5 μm in width, 500 μm in length, and the spacing between the fingers is 5 μm. The *I–V* curves of the device measured in dark and illumination conditions are shown in Fig. 4(b). The dark current of the device is as low as 145 pA at 10 V bias, while under the illumination of the 360 nm line of a Xenon lamp with the power density of 510 nW/cm^2, the current is 108 nA at 10 V bias, which means that under illumination many carriers have been generated. The above data reveals that the device can be employed to detect UV photons.

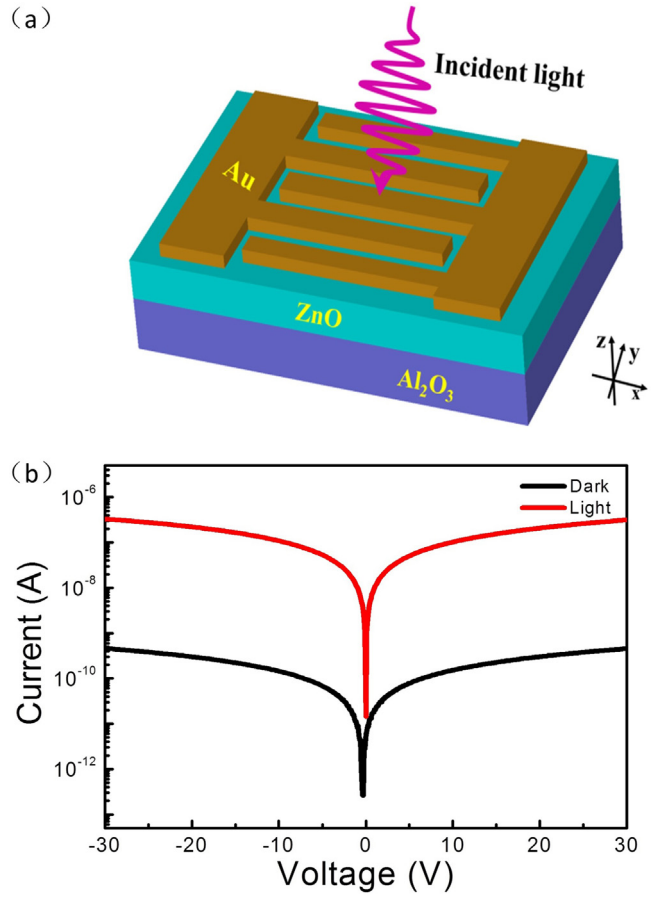

Fig. 4. (a) Schematic diagram of the device. (b) Dark current and photo current of the device under the UV illumination with power density of 510 nW/cm^2.

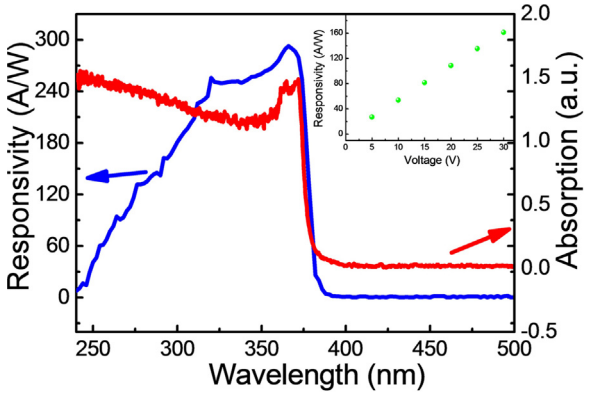

Fig. 5. (a) The responsivity and absorption spectrum of the photodetector fabricated from the ZnO:(Li,N) films. (b) Dependence of the responsivity of the photodetectors on the bias voltage.

Fig. 5 shows the response spectrum of the photodetector, and the absorption spectrum of the ZnO:(Li,N) films has also been displayed. From the absorption spectrum, a strong peak at around 370 nm is visible, which can be attributed to the excitonic absorption of ZnO, and the absorption in the UV region is strong, while that in the visible region is weak, which is favorable for UV photodetector fabricated from the films. The response spectrum of the device shows a broad peak centered at around 370 nm. The responsivity of the photodetector increases with the bias, and it can reach 287 A/W when the bias is 20 V.

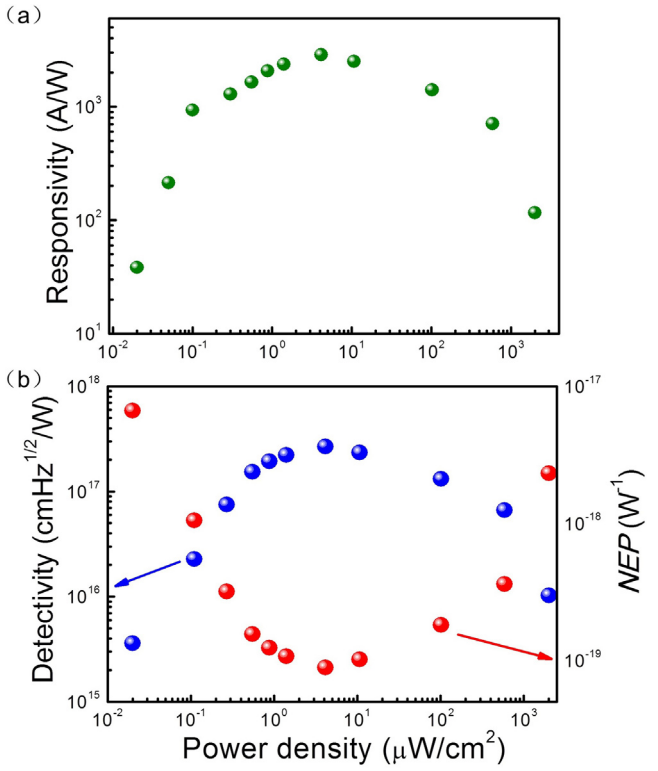

Fig. 6. (a) The relationship between the responsivity of the photodetector and the power density of the illumination source. (b) The dependence of the detectivity and *NEP* of the photodetectors on the power density of the illumination source.

Fig. 6(a) shows the relationship between the responsivity and the power density of the illumination source when the bias voltage is 20 V, it is obvious from the figure that when the power density of the illumination source is 2 mW/cm^2, the responsivity of the photodetector at 20 V is 116 A/W. The photodetector can still work when the power density of the illumination source is as low as 50 nW/cm^2, and the responsivity of the photodetector can reach 216 A/W at 20 V for the detection of such weak signals.

Detectivity (D^*) and noise equivalent power (*NEP*) are two important parameters that determine the performance of detecting weak signals for a photodetector. D^* and *NEP* of a photodetector can be expressed by the following formula [27]:

$$D* = R_\lambda (R_0/4KT)^{1/2} \quad (4)$$

$$NEP = A^{1/2}B^{1/2}D* \quad (5)$$

Here R_λ is the responsivity of the photodetector; R_0 is the dark impedance; A is the active area of the photodetector (5.75×10^{-4} cm^2 in our case); B is the bandwidth. Base on these two equations, the detectivity and *NEP* can be acquired. We note that the detectivity and *NEP* of the photodetector is strongly related to the power density of the illumination source, as shown in Fig. 6(b). The detectivity increases firstly and then decreases with the power density of the illumination source is increased. The detectivity and *NEP* of the photodetector at 20 V can reach 3.60×10^{15} cmHz$^{1/2}$/W and 6.67×10^{-18} W^{-1}, respectively, when the power density of the illumination source is reduced to 20 nW/cm^2, both of which are amongst the best values ever reported for ZnO based photodetectors, as illustrated in Table 3.

5. Conclusions

In conclusion, photodetectors that are capable of detecting weak signals have been developed from ZnO:(Li,N) films, and

Table 3
Comparison of the D^* and *NEP* of the photodetectors fabricated from the ZnO(Li:N) films with the reported values.

ZnO structure	D*(cmHz/W)	NEP(W^{-1})	Voltage (V)	Reference
Thin film	1.19×10^{10}	2.65×10^{-12}	5	[28]
Nanowall	3.38×10^{9}	1.87×10^{-10}	2	[29]
Nanorod	1.43×10^{15}	2.27×10^{-14}	5	[30]
Nanowire	2.13×10^{9}	5.83×10^{-13}	1.5	[31]
Nanoparticle	3.43×10^{15}	NA	9	[32]
Thin film	3.60×10^{15}	6.67×10^{-18}	20	This work

when the power density of the illumination source is as low as 20 nW, the detectivity and *NEP* of the photodetector can reach 3.60×10^{15} cmHz$^{1/2}$/W and 6.67×10^{-18} W^{-1}, both of which are amongst the best values ever reported for ZnO based photodetectors. The high-performance of the photodetector can be attributed to the relatively low carrier concentration of the ZnO:(Li,N) films caused by the compensation of the incorporated acceptors to the residual donors. The results reported in this paper may provide a route to ZnO photodetectors that is capable of detecting weak signals.

Acknowledgements

The authors would like to express our sincere appreciation to the kind help from Shanghai Synchrotron Radiation Facility (SSRF) and Beijing Synchrotron Radiation Facility (BSRF). This work is financially supported by the National Science Foundation for Distinguished Young Scholars of China (61425021), the Natural Science Foundation of China (11374296, U1604263, and 61604132), and the National Program for Support of Top-notch Young Professionals.

References

[1] R. Baraki, N. Novak, T. Frömling, T. Granzow, J. Rödel, Bulk ZnO as piezotronic pressure sensor, Appl. Phys. Lett. 105 (2014) 111604.
[2] D. Gedamu, I. Paulowicz, S. Kaps, O. Lupan, S. Wille, G. Haidarschin, Y.K. Mishra, R. Adelung, Rapid fabrication technique for interpenetrated ZnO nanotetrapod networks for fast UV sensors, Adv. Mater. 26 (2014) 1541.
[3] L. Peng, L. Hu, X. Fang, Low-dimensional nanostructure ultraviolet photodetectors, Adv. Mater. 25 (2013) 5321.
[4] J. Wang, X. Li, Y. Xia, S. Komarneni, H. Chen, J. Xu, L. Xiang, D. Xie, Hierarchical ZnO nanosheet-nanorod architectures for fabrication of poly(3-hexylthiophene)/ZnO hybrid NO2 sensor, ACS Appl. Mater. Interfaces 8 (2016) 8600.
[5] T. Tesfamichael, C. Cetin, C. Piloto, M. Arita, J. Bell, The effect of pressure and W-doping on the properties of ZnO thin films for NO2 gas sensing, Appl. Surf. Sci. 357 (2015) 728.
[6] S. Park, S. An, H. Ko, C. Jin, C. Lee, Synthesis of nanograined ZnO nanowires and their enhanced gas sensing properties, ACS Appl. Mat. Interfaces 4 (2012) 3650.
[7] J.N. Pei, D.Y. Jiang, M. Zhao, Q. Duan, R.S. Liu, L. Sun, Z.X. Guo, J.H. Hou, J.M. Qin, B.Z. Li, G.Y. Zhang, Controlled enhancement range of the responsivity in ZnO ultravioletphotodetectors by Pt nanoparticles, Appl. Surf. Sci. 389 (2016) 1056.
[8] H. Zhu, C.X. Shan, B. Yao, B.H. Li, J.Y. Zhang, Z.Z. Zhang, D.X. Zhao, D.Z. Shen, X.W. Fan, Y.M. Lu, Z.K. Tang, Ultralow-threshold laser realized in zinc oxide, Adv. Mater. 21 (2009) 1613.
[9] C.X. Wang, C. Zhu, C.Y. Lv, D.S. Li, X.Y. Ma, D.R. Yang, Electrically pumped random lasing from hydrothermal ZnO films of large grains, Appl. Surf. Sci. 332 (2015) 620.
[10] C. Soci, A. Zhang, B. Xiang, S.A. Dayeh, D.P.R. Aplin, J. Park, X.Y. Bao, Y.H. Lo, D. Wang, ZnO nanowire UV photodetectors with high internal gain, Nano Lett. 7 (2007) 1003.
[11] Y.Y. Lai, Y.P. Lan, T. Ch Lu, Strong light?matter interaction in ZnO microcavities, Light Sci Appl. 2 (2013) e76.
[12] Y.H. Lee, D.H. Kim, T.W. Kim, Enhanced current efficiency of organic light-emitting devices due to a broad localized surface plasmonic resonance of Au–ZnO nanocomposites, Appl. Surf. Sci. 355 (2015) 359.
[13] T.K. Lin, S.J. Chang, Y.K. Su, B.R. Huang, M. Fujita, Y. Horikoshi, ZnO MSM photodetectors with Ru contact electrodes, J. Cryst. Growth 281 (2005) 513.
[14] S.J. Young, L.W. Ji, S.J. Chang, X.L. Du, ZnO metal-semiconductor-metal ultraviolet photodiodes with Au contacts, J. Electrochem. Soc. 154 (2007) 26.
[15] N.N. Jandow, K. Ibrahim, H.A. Hassan, I–V characteristic for ZnO MSM photodetector with Pd contact electrodes on PPC plastic, AIP Conf. Proc. 1250 (2010) 424.
[16] H. Wang, G.B. Yi, X.H. Zu, P. Qin, M. Tan, H.S. Luo, Photoelectric characteristics of the p–n junction between ZnO nanorods and polyaniline nanowires and their application as a UV photodetector, Mater. Lett. 162 (2016) 83.
[17] H. Shen, C.X. Shan, B.H. Li, B. Xuan, D.Z. Shen, Reliable self-powered highly spectrum-selective ZnO ultraviolet photodetectors, Appl. Phys. Lett. 103 (2013) 232112.
[18] P. Fons, H. Tampo, A.V. Kolobov, M. Ohkubo, S. Niki, J. Tominaga, R. Carboni, F. Boscherini, S. Friedrich, Direct observation of nitrogen location in molecular beam epitaxy grown nitrogen doped ZnO, Phys. Rev. Lett. 96 (2006) 045504.
[19] S.Y. Tsai, M.H. Hon, Y.M. Lu, Local electronic structure of lithium-doped ZnO films investigated by X-ray absorption near-edge spectroscopy, J. Phys. Chem. C 115 (2011) 10252.
[20] J. Sharma, T. Gora, J.D. Rimstidt, R. Staley, X-ray photoelectron spectra of the alkali azides, Chem. Phys. Lett. 15 (1972) 232.
[21] J.S. Mrowiecka, V. Maurice, S. Zanna, L. Klein, P. Marcus, XPS study of Li ion intercalation in V2O5 thin films prepared by thermal oxidation of vanadium metal, Electrochim. Acta 52 (2007) 5644.
[22] H. Zhou, H.Q. Wang, X.X. Liao, Y. Zhang, J.C. Zheng, J.O. Wang, E. Muhemmed, H.J. Qian, K. Ibrahim, X. Chen, H. Zhan, J. Kang, Tailoring of polar and nonpolar ZnO planes on MgO (001) substrates through molecular beam epitaxy, Nanoscale Res. Lett. 7 (2012) 184.
[23] M. Newville, IFEFFIT: interactive XAFS analysis and FEFF fitting, J. Synchrotron Radiat. 8 (2001) 322.
[24] B. Ravel, M. Newville, ATHENA, ARTEMIS, HEPHAESTUS: data analysis for X-ray absorption spectroscopy using IFEFFIT, J. Synchrotron Radiat. 12 (2005) 537.
[25] B. Ravel, ATOMS: crystallography for the X-ray absorption spectroscopist, J. Synchrotron Radiat. 8 (2001) 314.
[26] H. Zhou, H.Q. Wang, Y. Li, K. Li, J.Y. Kang, J.C. Zheng, Z. Jiang, Y.Y. Huang, L.J. Wu, L.H. Zhang, K. Kisslinger, Y.M. Zhu, Evolution of wurtzite ZnO films on cubic MgO (001) substrates: a structural optical, and electronic investigation of the misfit structures, ACS Appl. Mater. Interfaces 6 (2014) 13823.
[27] H. Zhu, C.X. Shan, L.K. Wang, J. Zheng, J.Y. Zhang, B. Yao, D.Z. Shen, Metal-oxide-semiconductor-structured MgZnO ultraviolet photodetector with high internal gain, J. Phys. Chem. C 114 (2010) 7169.
[28] H.Y. Lee, Y.T. Hsu, C.T. Lee, ZnO-based resonant cavity enhanced metal–semiconductor–metal ultraviolet photodetectors, Solid State Electron. 79 (2013) 223.
[29] T.P. Chen, F.Y. Hung, S.P. Chang, S.J. Chang, S.L. Wu, Z.S. Hu, Noise properties of ZnO nanowalls deposited using rapid thermal evaporation technology, IEEE Photon. Technol. 25 (2013) 213.
[30] C.H. Chen, C.T. Lee, High detectivity mechanism of znO-Based nanorod ultraviolet photodetectors, IEEE Photon. Technol. Lett. 25 (2013) 348.
[31] H.B. Yu, E.A. Azhar, T. Belagodu, S. Lim, S. Dey, ZnO nanowire based visible-transparent ultraviolet detectors on polymer substrates, J. Appl. Phys. 111 (2012) 102806.
[32] F. Guo, B. Yang, Y. Yuan, Z. Xiao, Q. Dong, Y. Bi, J. Huang, A nanocomposite ultraviolet photodetector based on interfacial trap-controlled charge injection, Nat. Nanotechnol. 7 (2012) 798.